GEOPHYSICS, VOL. 66, NO. 5 (SEPTEMBER-OCTOBER 2001); P. 1471–1480, 9 FIGS., 2 TABLES.

Orbital vibrator seismic source for simultaneous *P*- and *S*-wave crosswell acquisition

Thomas M. Daley* and Dale Cox‡

ABSTRACT

A recently developed borehole seismic source, the orbital vibrator, was successfully deployed in a crosswell survey in a fractured basalt aquifer. This seismic source uses a rotating eccentric mass to generate seismic energy. Source sweeps with clockwise and counterclockwise rotations are recorded at each source location. Because this source generates circularly polarized waves, unique processing algorithms are used to decompose the recordings into two equivalent linearly oscillating, orthogonally oriented seismic sources. The orbital vibrator therefore generates *P*- and *S*-waves simultaneously for all azimuths. A coordinate rotation based on *P*-wave particle motion is used to align the source components from various depths. In a field experiment, both *P*- and *S*-wave arrivals were recorded using fluid-coupled hydrophone sensors. The processed field data show clear separation of *P*- and *S*-wave arrivals for in-line and crossline source components, respectively. A tensor convolutional description of the decomposition process allows for extension to multicomponent sensors.

INTRODUCTION

Crosswell seismic surveys have been used for subsurface imaging for more than 15 years (e.g., Mason, 1981; Peterson et al., 1985), with increased interest in recent years as acquisition hardware and analysis techniques have improved (see Hardage, 1992, for an overview). Field-data generation and collection have been predominantly focused on *P*-waves, and crosswell imaging (both tomographic imaging and reflection imaging) has mainly used *P*-waves. *S*-waves have been observed as mode conversions at reflecting interfaces and as *SV*-type waves generated by volumetric sources such as piezoelectric or explosive sources (Dong and Toksoz, 1995; Harris et al., 1995; Rector et al., 1995). There are clear advantages to using the extra information about material properties available if *S*-waves are consistently generated in a borehole simultaneously with *P*-waves.

One serious challenge about working with *S*-waves from volumetric sources is that *SV* arrivals near zero source-receiver offset are small (Van Schaack et al., 1995). The highest sensitivity is found for source-receiver angles near 45°. There have been efforts to develop a borehole *S*-wave source which would generate energy at a full range of source-receiver angles. In the early 1990s, Conoco, Inc. began development of a fluid-coupled borehole *S*-wave source known as an orbital vibrator. The orbital vibrator has an eccentric weight which rotates in the horizontal plane (for a vertical borehole). This type of source generates waves with circular polarization. The orbital vibrator technology was transferred to Lawrence Berkeley National Laboratory (LBNL) in 1996. Early work on the orbital vibrator was described in Hardage (1992). Conoco research teams successfully deployed the orbital vibrator at their fractured rock test facility (Liu et al., 1991, 1993). The orbital vibrator development and other potential applications for eccentric mass seismic sources are described by Cole (1997). We present here, for the first time, the unique processing steps required for the orbital vibrator and a field experiment demonstrating the use of an orbital vibrator with hydrophone sensors (previous studies had used clamped sensors).

In January 1998, LBNL used the orbital vibrator source for a crosswell survey in a fractured basalt aquifer at Idaho National Engineering and Environmental Laboratory's (INEEL) Test Area North (TAN) site. This was the first test of the orbital vibrator source in a hard rock (nonsedimentary) environment. We successfully acquired *P*-wave and *S*-wave arrivals using fluid-coupled hydrophone sensors. The use of fluid-coupled sensors had not previously been tested with an orbital vibrator, although *S*-waves generated by other sources have been observed with hydrophone sensors (e.g., Dong and Toksoz, 1995; Van Schaack et al., 1995). Using fluid-coupled sensors (along with the fluid-coupled orbital vibrator source) makes crosswell tomography surveys (both *P*- and *S*-wave) more efficient because of reduced acquisition time compared to using borehole clamping sources and sensors.

Manuscript received by the Editor June 18, 1999; revised manuscript received January 4, 2001.
*Lawrence Berkeley National Laboratory, University of California, 1 Cyclotron Road, M.S. 90-1116, Berkeley, California 94720. E-mail: tmdaley@lbl.gov.
‡Conoco Inc., 1000 South Pine Street, Ponca City, Oklahoma 74063. E-mail: v-dale.cox@usa.conoco.com.

SOURCE DESCRIPTION

There are currently two versions of the orbital vibrator in use at LBNL, an ac motor version and a dc motor version. The dc version was used in this study because it can use a standard wireline cable. The higher power ac version currently requires a special cable. The orbital vibrator uses an eccentric mass rotated about an axis by an electric motor. The expected radial displacement, using the center of the tool as origin in the horizontal plane, is shown in Figure 1. The motor is rotated at increasing frequency and then allowed to spin down to a stationary position. By rotating 360° about the vertical axis (Figure 1), the source generates a circularly polarized wavefront. The effective bandwidth for radiating seismic energy is approximately 70–400 Hz. The high-frequency limit is a function of the motor. Low-frequency energy is limited by the force available at low accelerations for a given mass. For this reason, there is typically a 0.5-s recording time delay after motor start for a 9-s sweep. Figure 2 shows a frequency versus time display of the orbital vibrator output as measured by an accelerometer mounted radially on the source case. For each source location a clockwise (cw) and a counterclockwise (ccw) rotation is generated. The motor is not under feedback control of phase and amplitude like a surface seismic vibrator source; therefore, each sweep has a unique phase and amplitude spectrum. The source monitor accelerometer signal is used for phase and amplitude deconvolution of sensor data recordings for each sweep. The phase deconvolution corrects for variable angular offset of the eccentric mass relative to the monitor accelerometer, which is otherwise seen as phase shifts in the sensor data. We have a consistent coordinate system for deconvolution of cw and ccw rotations because the outer shell of the source (to which the monitor accelerometer is attached) is held fixed by the armored wireline cable. Standard wireline cable has two wraps of steel armor with opposite orientations (cw and ccw), thereby resisting torque and maintaining a consistent coordinate system for each source depth. Moving the source between depths can cause cable rotation and a change of the coordinate system.

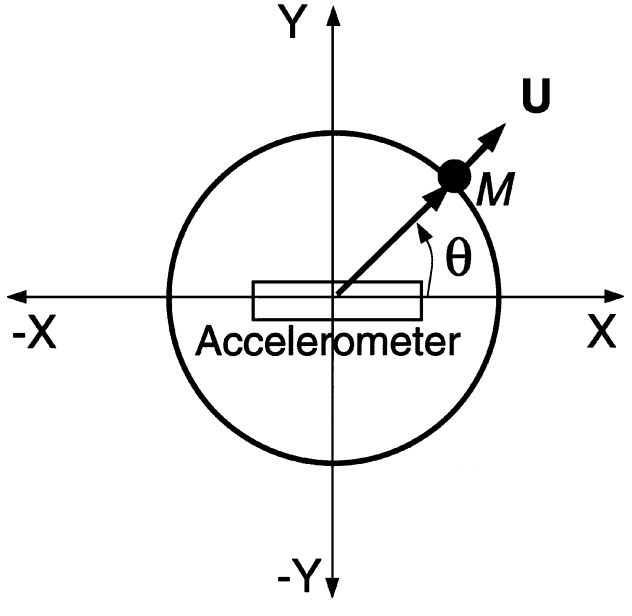

FIG. 1. Schematic model of orbital vibrator. Eccentric mass is represented by its center of mass M rotated in the horizontal plane. The coordinate system origin is the center of the downhole source. The x-axis is defined by the orientation of an accelerometer mounted on the nonrotating frame of the source. The angle θ is measured from the x-axis to M. The center of mass has a radial displacement **u**.

Why deconvolution instead of correlation?

The orbital vibrator, like the surface vibrator, has a long sweep. Some method is needed to compress the sweep and increase the signal-to-noise ratio. The linear sweep source signal $\mathbf{s}(f)$ usually used for a surface vibrator has a constant amplitude spectrum so the autocorrelation has a flat bandpass. For a rotating mass, the radial acceleration is $r\omega^2$, where r is the radial distance from the origin to the mass. Using this model, the sweep from the orbital vibrator has an acceleration spectrum which increases as the square of the frequency, and recordings of the source monitor accelerometer have confirmed this relationship. Thus the autocorrelation of the orbital vibrator monitor signal has an amplitude spectrum which increases as the fourth power of the frequency. This tends to give a wavelet with pronounced side lobes. One solution to this side lobe problem is to do a signature deconvolution instead of correlation. Thus, in the frequency domain, we divide by $\mathbf{s}(f)$ instead of multiplying by $\mathbf{s}^*(f)$, the complex conjugate of $\mathbf{s}(f)$. This step compresses the signal and reduces the side lobes in the data. To guard against dividing by zero, a suitable diagonal load (random noise addition) is used.

Unlike the surface vibrator, no provision is made to ensure the eccentric mass starts in the same position relative to the sensor on the source. This means that each sweep, clockwise or counterclockwise, starts from an arbitrary angle. This arbitrary angle introduces an arbitrary phase in $\mathbf{s}(f)$ which is measured by both the source sensor and the receivers and is automatically eliminated by either correlation or deconvolution.

In addition, the orbital vibrator source sweep does not exactly repeat itself from shot to shot. However, the sensor on the source always measures the source motion, so that after deconvolution, the resultant deconvolved source signature is repeatable enough to allow stacking.

DECOMPOSITION OF CIRCULAR POLARIZATION INTO LINEAR POLARIZATION

To recover equivalent linearly polarized waves from the circularly polarized waves, both cw and ccw rotations are used. Assuming the source eccentric mass motion is described by the motion of its center of mass in the horizontal plane, we can describe both cw and ccw source motions in rectangular coordinates. In the horizontal plane, we take the x-axis to be aligned with the monitor accelerometer, the y-axis to be normal to the accelerometer, and the angle θ to be measured from the x-axis to the center of mass (as shown in Figure 1). For a generalized source function $\mathbf{s}(f)$, where the eccentric mass is rotating at a frequency $f = \omega/2\pi$, then the angle $\theta = \omega t$ (see Table 1 for symbols). Assuming radial displacement **u** at the center of mass location, the x- and y-components of displacement (u_x and u_y) can be related to θ for cw and ccw motion.

Let u_{cwx} and u_{cwy} be the x- and y-components of $\mathbf{u_{cw}}$ (cw displacement), and let u_{ccwx} and u_{ccwy} be the x- and y-components of $\mathbf{u_{ccw}}$ (ccw displacement). We assume that the displacement $\mathbf{u}$ has equal amplitude A for all θ. We then have the following relations:

$$u_{cwx} = A\cos(\theta), \tag{1}$$

$$u_{cwy} = A\sin(\theta), \tag{2}$$

$$u_{ccwx} = A\cos(-\theta) = A\cos(\theta), \tag{3}$$

$$u_{ccwy} = A\sin(-\theta) = -A\sin(\theta). \tag{4}$$

We now combine recorded data for cw and ccw rotations to generate the data equivalent to linear source motion $u_x(\omega t)$ and $u_y(\omega t)$.

To obtain $u_x(\omega t)$, we add the cw and ccw recordings:

$$\begin{aligned} u_x(\omega t) &= \mathbf{u_{cw}} + \mathbf{u_{ccw}} \\ &= u_{cwx} + u_{cwy} + u_{ccwx} + u_{ccwy} \\ &= A\cos(\omega t) + A\sin(\omega t) + A\cos(\omega t) - A\sin(\omega t) \\ &= 2A\cos(\omega t). \end{aligned} \tag{5}$$

Similarly, to recover the y-component motion, we subtract the cw and ccw recordings:

$$\begin{aligned} u_y(\omega t) &= \mathbf{u_{cw}} - \mathbf{u_{ccw}} \\ &= u_{cwx} + u_{cwy} - u_{ccwx} - u_{ccwy} \\ &= A\cos(\omega t) + A\sin(\omega t) - A\cos(\omega t) + A\sin(\omega t) \\ &= 2A\sin(\omega t). \end{aligned} \tag{6}$$

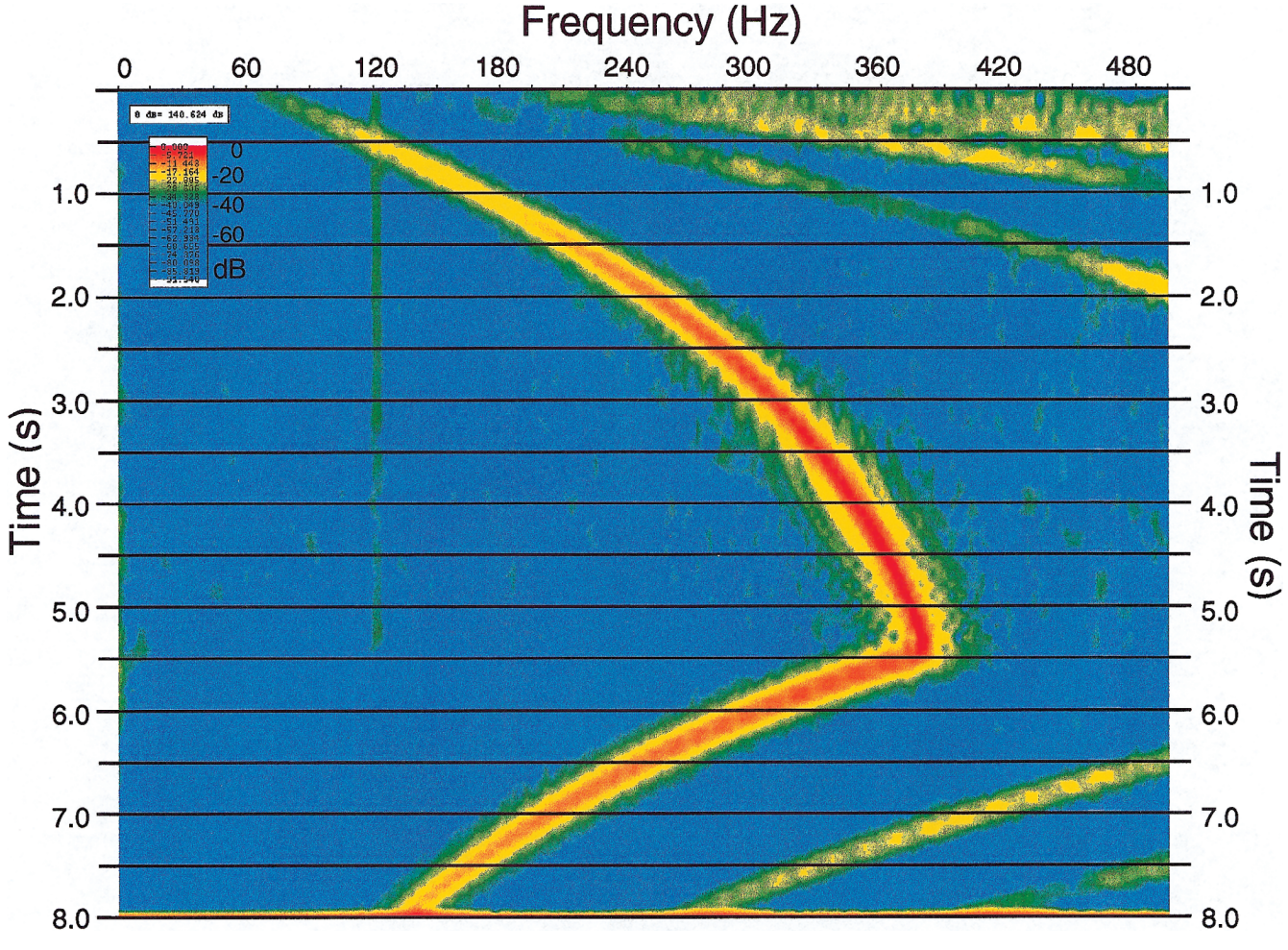

FIG. 2. Frequency versus time display of orbital vibrator sweep as measured by monitor accelerometer mounted on the source. Acceleration amplitude in decibels relative to the maximum is displayed using color scale in the upper left corner. Time is recorded time, the first 0.5 s of the sweep is not recorded and not shown here. At the begining of recording, the sweep frequency is about 70 Hz and increases to about 400 Hz at 5.5 s, at which time the motor is switched off and the sweep reduces frequency to about 120 Hz at 8.0 s, when recording is stopped. Accelerations within 20 dB of maximum are recorded from about 100 to 400 Hz. A deconvolution is used to correct for the amplitude variation. Also visible is 120 Hz powerline noise and higher harmonics of the main sweep (e.g., between 240 and 480 Hz and from 0.5 to 2.0 s).

A schematic drawing of the motion represented by equations (5) and (6) is shown in Figure 3. Because the two linearized components of motion u_x and u_y have a phase difference, a Hilbert transform (90° phase shift) of u_y data is used to correct the phase difference. The circularly polarized cw and ccw recordings are thus decomposed into equivalent linear x- and y-polarized source recordings. For this model of the orbital vibrator, we have independent sources oscillating sinusoidally along the x- and y-axis. For a sensor aligned with the x-axis in a homogeneous media, the u_x source data will contain longitudinal P-wave motion and the u_y source data will contain SH-type S-wave motion. A more detailed tensor convolutional description of the decomposition, including multicomponent sensors, is in Appendix A.

ROTATION USING PARTICLE MOTION

The x, y coordinate system used above can change for each source depth because the wireline cable allows rotation about the vertical axis when the cable is moved up or down the well. A coordinate system based on the source monitor accelerometer (as shown in Figure 1) is potentially different for each depth. However, we can use the received P-wave particle motion to define a consistent source coordinate system at each depth, neglecting local anisotropy. By requiring that u_x be aligned with the P-wave particle motion for all source depths, we define a new coordinate system. For crosswell data in 1-D isotropic media, this coordinate system will have u_x and u_y correctly aligned for all source depths. This procedure is equivalent to the coordinate system rotation used for three-component borehole sensors in crosswell and vertical seismic profile (VSP) surveys, except that we are compensating for source rotation instead of receiver rotation. We calculate the rotation angle using the eigenvectors (λ_1 and λ_2) of the covariance matrix, $\mathbf{\Phi}$, for data in the P-wave arrival window (Kanasewich, 1981), where

$$\mathbf{\Phi} = \begin{pmatrix} \Phi_{xx} & \Phi_{xy} \\ \Phi_{yx} & \Phi_{yy} \end{pmatrix}, \tag{7}$$

and

$$\Phi_{xy} = \frac{1}{N} \sum_{i=1,N} [(x_i - \mu_x)(y_i - \mu_y)], \tag{8}$$

where μ_x = mean of x_i and μ_y = mean of y_i, for N values of x_i and y_i, which are values of the windowed u_x and u_y seismograms (the decomposed data).

In practice, multiple sensors are recorded for each source (a shot gather), so a weighted average of the individual sensor rotation angles calculated for each shot gather is used. The weighting parameter we use is the particle motion linearity, $F(\lambda_1, \lambda_2) = 1 - (\lambda_2/\lambda_1)$ which varies between 1 (linear polarization) and 0 (circular polarization) (Kanasewich, 1981).

This rotation completes the initial data processing for single component, omnidirectional receivers like the hydrophones used in our study. After this step, we have transformed to an in-line data set (all sources with aligned x-component) and a cross-line data set (all sources with aligned y-component). The summarized processing flow is shown in Figure 4. When a directional receiver is used, which can rotate independent of the source, a second data rotation is necessary to provide a consistent receiver orientation. A discussion of the tensor processing for multicomponent directional receivers is in Appendix B.

Table 1. Symbols used in the text.

Symbol	Description
r	Radial distance from origin to eccentric mass
ω	Angular frequency
f	Frequency
$\mathbf{s}$	Source sweep signal vector
θ	Angle (counter clockwise from x-axis) to eccentric mass
x, y	Cartesian coordinates
$\mathbf{u}$	Vector displacement of eccentric mass
cw	Clockwise
ccw	Counterclockwise
A	Amplitude of radial source displacement
t	Time
u_x, u_y	x- and y-components of $\mathbf{u}$
$\mathbf{u_{cw}}$, $\mathbf{u_{ccw}}$	Vector displacement for cw and ccw eccentric mass rotation
u_{cwx}, u_{cwy}	x- and y-component of displacement for cw rotation
u_{ccwx}, u_{ccwy}	x- and y-component of displacement for ccw rotation
$\mathbf{\Phi}$	Covariance matrix of recorded receiver data
Φ_{xy}, Φ_{xy}, Φ_{yx}, Φ_{yy}	Scalar components of $\mathbf{\Phi}$
μ_x, μ_y	Mean of N values of u_x and u_y data in a time window
λ_1, λ_2	First (largest), and second eigenvalue of $\mathbf{\Phi}$
F	Particle motion linearity function

FIELD EXPERIMENT

The orbital vibrator was deployed at the INEEL TAN site in January 1998 as part of site characterization activities. The lithology is multiple thin (5–10 m) basalt flows with fractures, vesicles, and occasional sedimentary interbeds. The site is in the Snake River Plain Aquifer, with a static water level depth of approximately 64 m. An overview of ground water remediation activities at the TAN site including seismic tomography is available in an INEEL report (Bukowski and Sorenson, 1998). Orbital vibrator data was recorded at 0.5-m source intervals from 66 to 100 m below ground level in well TAN-37. The hydrophone sensors were placed every 0.5 m from 65.5 to 93 m in well TAN-25. Seven sensors were recorded for each source sweep, and source and sensors were moved to provide full source/receiver coverage. The survey geometry is shown in Figure 5. An example field recording of multiple source depths for a single receiver after deconvolution is shown in Figure 6a. The same field data after decomposition and rotation is shown in Figures 6b and 6c, respectively. In addition to the processing steps described above, notch filters were used at 60, 121, 181, and 303 Hz to remove powerline noise.

The decomposition and rotation processing separates the recorded data into two seismograms for each source-receiver pair: an in-line and a cross-line source component. Theoretically, this processing will separate the *P*-wave and *S*-wave energy onto the in-line and cross-line components, respectively. The decomposed, rotated recordings of Figure 6c do show good separation of *P*- and *S*-waves between these components. Notice that in Figure 6b, the *P*-wave energy at about 10 ms and the *S*-wave energy at about 20 ms are present on both *x* and *y* components. Comparing Figures 6b and 6c, we see most of the shear-wave energy in Figure 6b (at about 20 ms on both components) is moved to the cross-line component of Figure 6c. The separation of shear-wave energy was accomplished by rotation analysis of a time window encomposing the *P*-wave arrival only.

Identification of *P*- and *S*-waves is accomplished by observing the distribution of energy between in-line and cross-line components and by the comparison of traveltimes with those expected for basalt velocities. The *P*-wave traveltimes of about 10 ms on the in-line component shown in Figure 6c correspond to a velocity of 4 km/s. The *S*-wave traveltimes of about 20 ms on the cross-line component shown in Figure 6c correspond to a velocity of 2 km/s. These velocities are in agreement with published velocities for basalt (Carmichael, 1982).

Note that this relatively good data quality was obtained at a field site which is notably more complex than the simple models used to describe the analysis algorithms, thus indicating the robustness of the technique. At this point, the data are ready for traveltime or amplitude analysis of both *P*- and *S*-waves, an analysis not in the scope of this paper. It is notable that because the source is cylindrically symmetric, data equivalent to Figure 6 could be simultaneously acquired from receiver wells on any azimuth, again increasing acquisition efficiency.

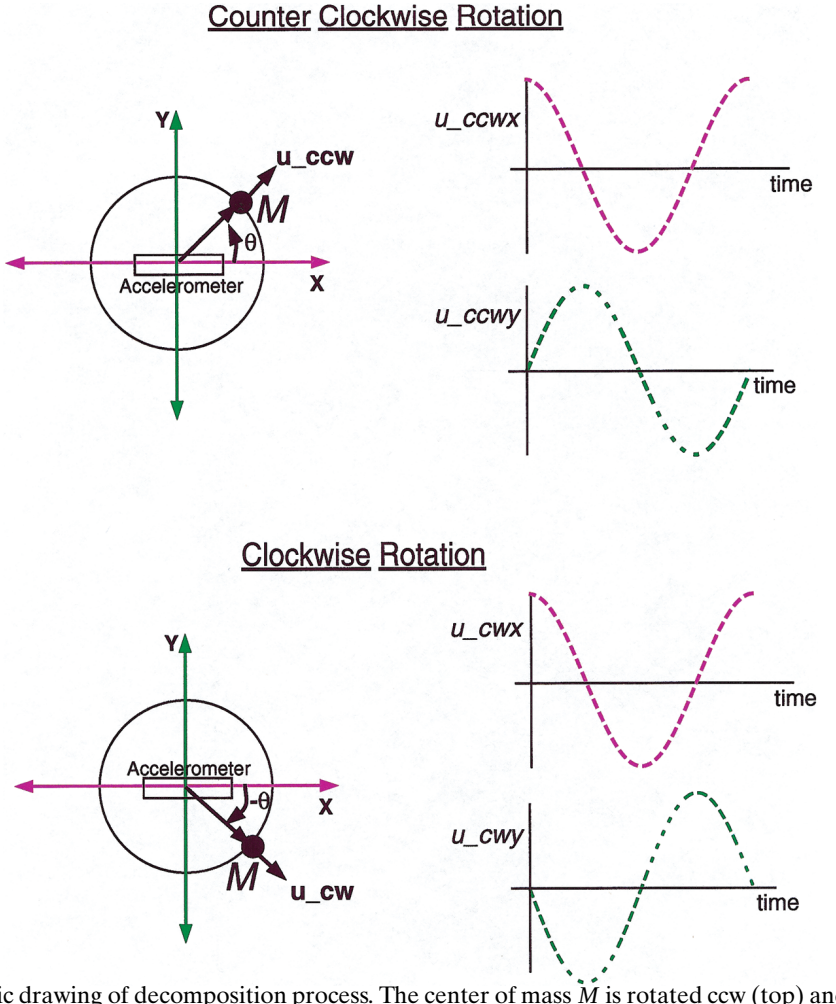

FIG. 3. Schematic drawing of decomposition process. The center of mass *M* is rotated ccw (top) and cw (bottom) causing a displacement **u** which has *x* and *y* components (shown in purple and green, respectively, on the right-side graphs). The summing of ccw rotation recordings (top) and cw rotation recordings (bottom) produces sinusoidal motion on the *x*-axis while canceling motion on the *y*-axis. Similarly, subtraction of cw rotation recordings from ccw recordings produces sinusoidal motion on the *y*-axis while canceling motion on the *x*-axis. The two perpendicular directions of motion (*x* and *y*) differ in phase by 90°; therefore, a phase shift is applied to one of the decomposed data sets to give equivalent *x* and *y* data.

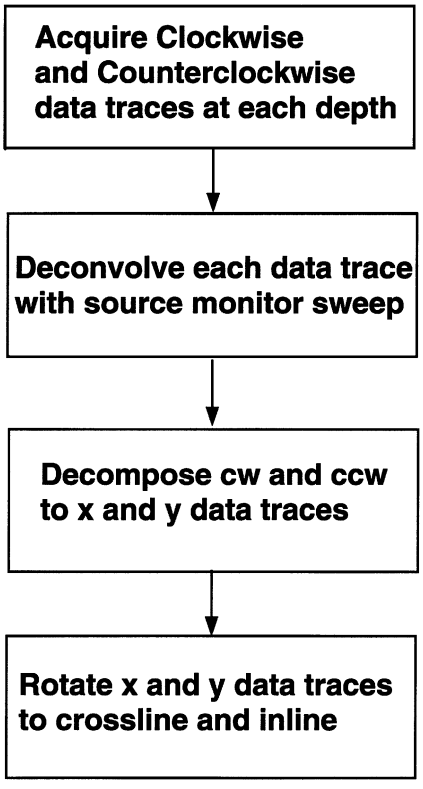

FIG. 4. Block diagram of processing steps for orbital vibrator data. Details of each step are described in the accompanying text.

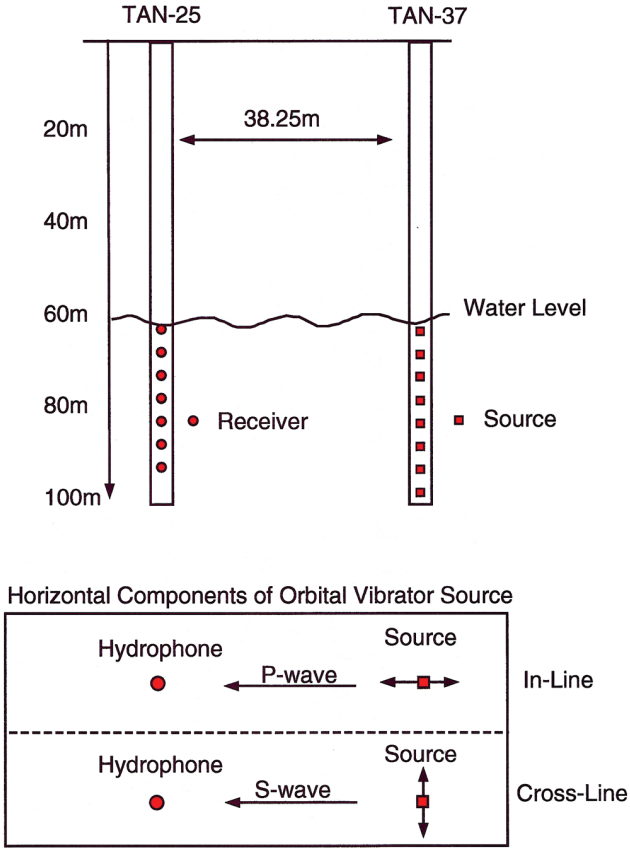

FIG. 5. Geometry of crosswell field data collected at INEEL TAN site (top) with orbital vibrator source components in plan view (bottom). The two components of motion obtained from the orbital vibrator source allow separation of *P*- and *S*-wave energy as shown in Figure 6c. All data was collected between 65.5 and 100 m, which is below the water table (at about 64 m), with source and receiver spacing of 0.5 m. The well spacing of 38.25 m is slightly more than the maximum vertical sampling of 34.5 m.

SUMMARY

We have shown how an eccentric mass orbital vibrator can be used to simultaneously generate *P*- and *S*-waves. Unique processing algorithms are used to decompose cw and ccw circularly polarized waves into equivalent linearly polarized waves. The orthogonal linear source components are rotated into a consistent source-receiver coordinate system using particle motion eigenvector analysis.

A field data example demonstrates the function of this seismic source using omnidirectional, fluid-coupled hydrophone sensors. Simultaneous acquisition of *P*- and *S*-wave properties with efficient fluid coupled source and sensors has great potential for extending geophysical investigations which were previously limited to *P*-wave data. As more extensive three-component sensor acquisition is now possible, the extension of the orbital vibrator processing steps to multicomponent sensors allow vector wave analysis such as *S*-wave splitting studies.

ACKNOWLEDGMENTS

Thanks to John Stock of Conoco; Ken Williams, Don Lippert, and Cecil Hoffpauir of LBNL; and Chad Hersley of INEEL for help with the dc orbital vibrator and the field data acquisition. Thanks to Ernie Majer of LBNL for discussions and support of this work. This work was supported by the Office of the Deputy Secretary, Assistant Secretary of Environmental Management, and by the Assistant Secretary for Fossil Energy, Federal Energy Technology Center, and by the Assistant Secretary for Fossil Energy, Office of Natural Gas and Petroleum Technology, under the Natural Gas and and Oil Technology Partnership program, all of the U.S. Department Energy under Contract No. DE-AC03-76SF00098. Data processing performed at the Center for Computational Seismology supported by the Associate Director of the Office of Basic Energy Sciences, Division of Engineering and Geosciences, of the U.S. Department of Energy, also under Contract No. DE-AC03-76SF00098.

REFERENCES

Bukowski, J. M., and Sorenson, Jr., K. S., Site conceptual model: 1996 activities, data analysis, and interpretation, Test Area North operable Unit 1-07B: Idaho National Engineering Laboratory INEL/EXT-97-00556.

Carmichael, R. S., 1982, Handbook of physical properties of rocks, vol. 2; CRC Press, Inc.

Cole, J. H., 1997, The orbital vibrator, a new tool for characterizing interwell reservoir space, The Leading Edge, **16**, 281–283.

Dong, W., and Toksoz, M. N., 1995, Borehole seismic-source radiation in layered isotropic and anisotropic media: Real data analysis: Geophysics, **60**, 748–757.

Hardage, B. A., 1992, Crosswell seismology and reverse VSP: Geophysical Press.

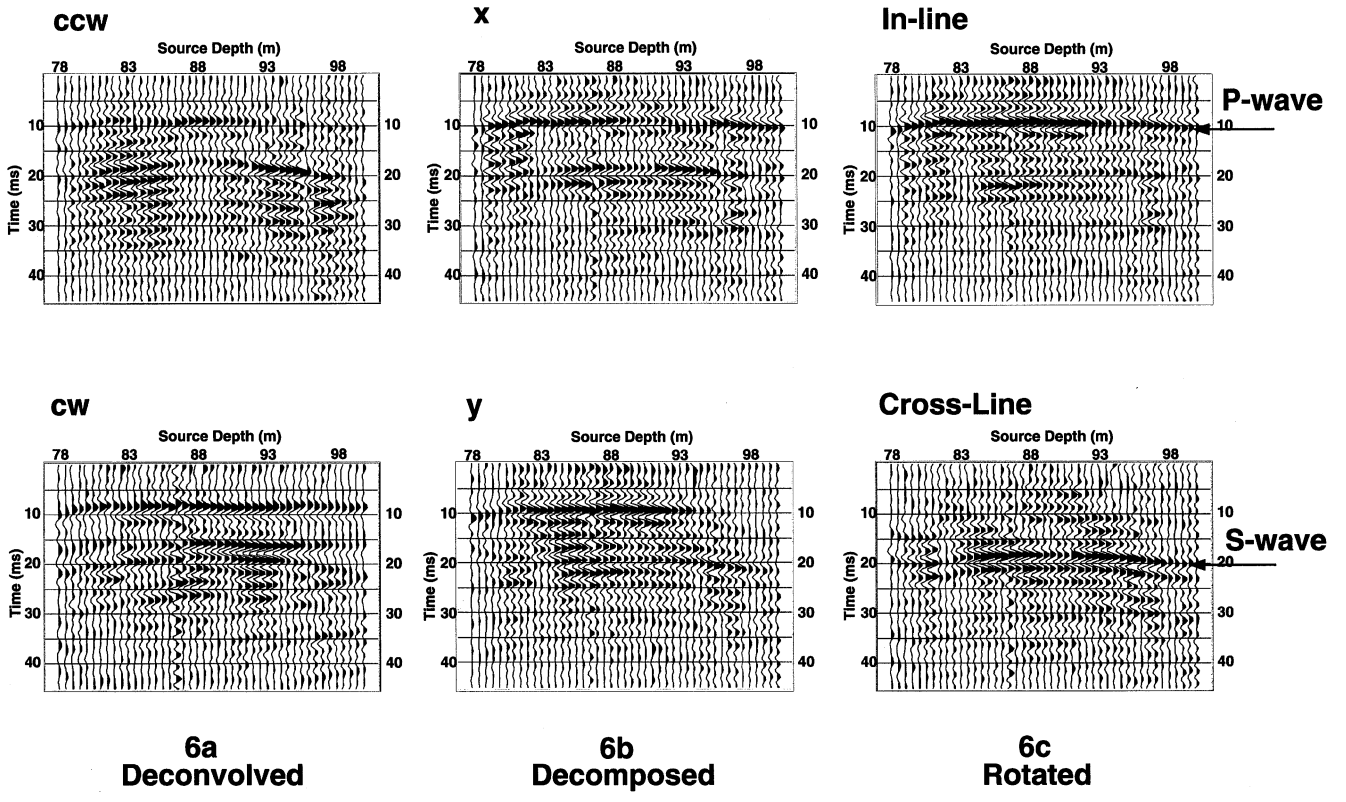

FIG. 6. A field data example showing the processing steps for orbital vibrator data. The data is a common receiver gather from a hydrophone receiver at 88 m depth for sources from 78 to 100 m depths. Shallower recordings are not shown because an intense fracture zone caused disruption of waveforms. (a) The counterclockwise (top) and clockwise (bottom) recordings after source signature deconvolution. (b) The x and y components after decomposition. (c) The in-line and cross-line components after particle motion based rotation. The traces in each panel are normalized to the maximum of the panel. The rotated result in (c) shows good separation between the *P*-wave arrival at about 10 ms in the in-line data and the *S*-wave arrival at about 18 ms in the cross-line data, thus demonstrating the simultaneous generation of *P*- and *S*-waves.

Harris, J. M., Nolen-Hoeksema, R. C., Langan, R. T., Van Schaack, M., Lazaratos, S. K., and Rector III, J. W., 1995, High-resolution crosswell imaging of a West Texas carbonate reservoir: Part 1—Project summary and interpretation, Geophysics, **60**, 667–681.

Kanasewich, E. R., 1981, Time sequence analysis in geophysics: Univ. of Alberta Press.

Liu, E., Crampin, S., and Queen, J. H., 1991, Fracture detection using reverse vertical seismic profiles and cross-hole surveys at the Conoco Borehole Test Facility, Oklahoma: Geophys. J. Internat., **107**, 449–463.

Liu, E., Crampin, S., Queen, J. H., and Rizer, W. D., 1993, Velocity and attenuation anisotropy caused by microcracks and macrofractures in a azimuthal reverse VSPs: Canadian J. Expl. Geophys., **29**, 177–188.

Mason, I. M., 1981, Algebraic reconstruction of a two-dimensional velocity inhomogeneity in the High Hazles seam of Thoresby colliery: Geophysics, **46**, 298–308.

Peterson, J. E., Paulsson, B. N. P., and McEvilly, T. V., 1985, Applications of algebraic reconstruction techniques to crosshole seismic data: Geophysics, **50**, 1566–1580.

Rector III, J. W., Lazaratos, S. K, Harris, J. M., and Van Schaack, M, 1995, High-resolution crosswell imaging of a West Texas carbonate reservoir: Part 3—Wavefield separation of reflections: Geophysics, **60**, 692–701.

Van Schaack, M., Harris, J. M., Rector III, J. W., and Lazaratos, S. K., 1995, High-resolution crosswell imaging of a West Texas carbonate reservoir: Part 2—Wavefield modeling and analysis: Geophysics, **60**, 682–691.

APPENDIX A
TENSOR CONVOLUTIONAL DERIVATION OF DECOMPOSITION

In order to discuss more generally how data from an orbital vibrator should be processed to allow for multicomponent sensors, we use a tensor convolutional description and extend the use of the convolution assumption from the scalar case to the tensor case (see Table A-1 for symbols). The usual statement of the scalar convolution assumption in the frequency domain is

$$R(f) = \mathrm{T}(f)\,\mathrm{s}(f),$$

where $R(f)$ is the signal detected by the receiver, $\mathrm{T}(f)$ is the earth response, and $s(f)$ is the input sweep (source wavelet).

With a vibrating source, we need to compress the wavelet from a long sweep to a shorter pulse to increase the signal-to-noise ratio; thus, correlation is used. The processed signal is

$$\mathrm{C}(f) = \mathrm{R}(f)\mathrm{s}^*(f) = \mathrm{T}(f)\mathrm{s}(f)\mathrm{s}^*(f),$$

where $\mathrm{C}(f)$ is the correlated signal detected by the receiver and $s^*(f)$ is the complex conjugate of the input sweep; $\mathrm{s}(f)\mathrm{s}^*(f)$ is a band-limited spike. To simplify our equations, we will assume $\mathrm{s}(f)\mathrm{s}^*(f) = 1$, thus

$$\mathrm{C}(f) = \mathrm{T}(f).$$

Consider an experiment using the usual *S*-wave (*SH*) acquisition geometry. Figure A-1 shows a source oriented in the *y*-direction with receivers oriented in both the *x*- and *y*-directions. For this experiment, the tensor description of the convolution assumption is

$$\begin{aligned} R_x(f) &= T_{xy}(f)\mathrm{s}_y(f) \\ R_y(f) &= T_{yy}(f)\mathrm{s}_y(f), \end{aligned} \qquad \text{(A-1)}$$

where subscripts have been added to the matrix **R** and the vector **s** to indicate their orientation. $T_{xy}(f)$ is the earth response in the *x*-direction for a source in the *y*-direction, and $T_{yy}(f)$ is the earth response in the *y*-direction for a source in the *y*-direction.

Table A-1. Additional symbols used in appendices.

Symbol	Description
f	Frequency
R	Recorded receiver signal matrix
T	Earth response matrix
s	Source sweep signal vector
s^*	Complex conjugate of **s**
C	Correlated receiver signal matrix
R_x, R_y	*x*- and *y*-components of **R**
s_x, s_y	*x*- and *y*-components of **s**
T_{ij}	ij components of **T** where i and $j = x, y,$ or z
C_{xx}, C_{xy}, C_{yx}, C_{yy}	*x* and *y* components of matrix **C**
C_{x+}, C_{y+}	*x* and *y* components of matrix **C** for ccw source rotation
C_{x-}, C_{y-}	*x* and *y* components of matrix **C** for cw source rotation
x', y'	Coordinates defined by the source monitor sensor
θ	Angle between source monitor sensor and receiver sensor

Now consider an experiment used to acquire *S*-wave (*SV*) data. Figure A-2 shows a source oriented in the *x*-direction with receivers oriented in both the *x*- and *y*-directions. In this case,

$$\begin{aligned} R_x(f) &= T_{xx}(f)s_x(f) \\ R_y(f) &= T_{yx}(f)s_x(f), \end{aligned} \qquad \text{(A-2)}$$

where $T_{xx}(f)$ is the earth response in the *x*-direction for a source in the *x*-direction, and $T_{yx}(f)$ is the earth response in the *y*-direction for a source in the *x*-direction. In general, T_{xy} is not equal to T_{yx}.

If a vibratory source is used, then the result of correlation for the *SH* experiment is

$$C_{xy}(f) = R_{xy}(f)s_y^*(f) = T_{xy}(f)s_y(f)s_y^*(f) = T_{xy}(f)$$

$$C_{yy}(f) = R_{yy}(f)s_y^*(f) = T_{yy}(f)s_y(f)s_y^*(f) = T_{yy}(f),$$

and for the *SV* experiment is

$$C_{xx}(f) = R_{xx}(f)s_x^*(f) = T_{xx}(f)s_x(f)s_x^*(f) = T_{xx}(f)$$

$$C_{yx}(f) = R_{yx}(f)s_x^*(f) = T_{yx}(f)s_x(f)s_x^*(f) = T_{yx}(f),$$

where we have assumed $s_y(f)s_y^*(f)$ and $s_x(f)s_x^*(f)$ are both equal to one. Thus, with the usual acquisition methods, the tensor earth response function can be recovered.

The discussion so far has used two dimensions, but it can be easily extended to the three-dimensional case. In that case,

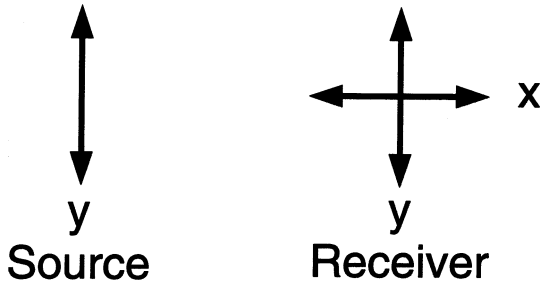

FIG. A-1. A typical *SH*-wave experiment. Source oriented in the *y*-direction is recorded by receivers oriented in the *x* and *y*-directions.

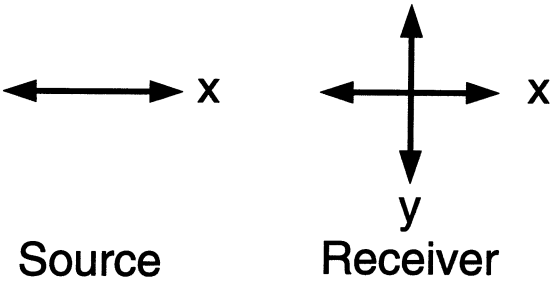

FIG. A-2. A typical *SV*-wave experiment. Source oriented in the *x*-direction is recorded by receivers oriented in the *x*- and *y*-directions.

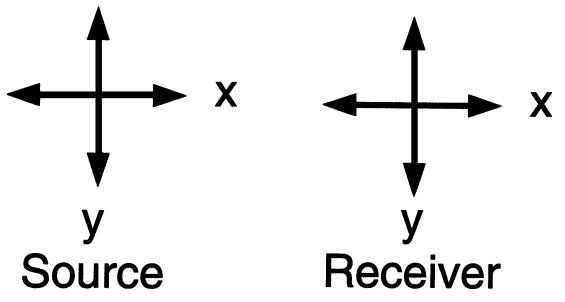

FIG. A-3. The general experiment. Sources oriented in both the x- and y-directions are recorded by receivers oriented in the x- and y-directions.

the quantities **C** and **T** are 3×3 matrices and **s** is a three-dimensional vector. We will continue to use two-dimensional analysis mindful that everything can be extended to three dimensions.

Any real source will not produce a force along a single direction, but will produce forces in all directions simultaneously, as shown in Figure A-3. In this case, by simply adding equation (A-1) and equation (A-2) from the two separate experiments described above, we have

$$\begin{aligned} R_x(f) &= T_{xx}(f)s_x(f) + T_{xy}(f)s_y(f) \\ R_y(f) &= T_{yx}(f)s_x(f) + T_{yy}(f)s_y(f). \end{aligned} \tag{A-3}$$

In particular, we see from Figure 3 that the orbital vibrator produces forces in the x- and y-directions that are related by a 90° phase rotation. Thus $s_x(f)$ and $s_y(f)$ are not independent but are related, for a ccw rotation, by

$$s_y(f) = s_x(f)\exp(i\pi/2) = is_x(f),$$

where $i = \sqrt{-1}$. Using this relationship in equations (A-3), they become

$$\begin{aligned} R_x(f) &= (T_{xx}(f) + iT_{xy}(f))s_x(f) \\ R_y(f) &= (T_{yx}(f) + iT_{yy}(f))s_x(f). \end{aligned} \tag{A-4}$$

After correlation and assuming $s_x(f)s_x^*(f)$ is one, we have

$$\begin{aligned} C_{x+}(f) &= T_{xx}(f) + iT_{xy}(f) \\ C_{x+}(f) &= T_{yx}(f) + iT_{yy}(f). \end{aligned} \tag{A-5}$$

The + subscript denotes ccw rotation. Notice that T_{xx}, T_{xy}, T_{yx}, and T_{yy} cannot be independently determined by these two equations, only certain linear combinations are determined. Just as in the *SH*- and *SV*-case, two experiments are necessary to find the full tensor response.

The second experiment is accomplished by a cw rotation of the source. For a cw rotation, since the phase rotation is -90°, we have

$$s_y(f) = -is_x(f).$$

Using this equation in the general relationship in equations (A-3) above and correlating, we get

$$\begin{aligned} C_{x-}(f) &= T_{xx}(f) - iT_{xy}(f) \\ C_{x-}(f) &= T_{yx}(f) - iT_{yy}(f), \end{aligned} \tag{A-6}$$

where the + and − subscripts refer to ccw and cw rotations, respectively. By adding and subtracting equations (A-5) and equations (A-6) we can derive

$$\begin{aligned} T_{xx}(f) &= (C_{x+}(f) + C_{x-}(f))/2, \\ T_{xy}(f) &= -i(C_{x+}(f) - C_{x-}(f))/2, \\ T_{yx}(f) &= (C_{y+}(f) + C_{y-}(f))/2, \\ T_{yy}(f) &= -i(C_{y+}(f) - C_{y-}(f))/2. \end{aligned} \tag{A-7}$$

The factor −i in equations (A-7) accounts for the 90° phase rotation discussed in the text.

APPENDIX B
TENSOR ROTATION FOR SOURCE AND MULTICOMPONENT RECEIVERS

The previous analysis in Appendix A assumes that the signal $s_x(f)$ can be measured. In practice, the sweep is measured by a sensor fixed to the case of the orbital vibrator. As the source is moved in the borehole, the case rotates relative to some fixed direction. At any particular level, assume the sensor is located at an angle θ relative to the fixed axis used above. Then, for a ccw rotation of the source,

$$\begin{aligned} \mathbf{s}(\theta) &= s_x\cos(\theta) + s_y\sin(\theta), \\ &= s_x\cos(\theta) + is_x\sin(\theta), \\ &= s_x(\cos(\theta) + i\sin(\theta)), \\ &= s_x\exp(i\theta), \end{aligned} \tag{B-1}$$

where $s_y(f) = is_x(f)$ has been used. Thus, the measured signal $\mathbf{s}(\theta)$ is simply a phase rotation of s_x by an angle θ. For a cw rotation of the source, since $s_y(f) = -is_x(f)$, we get $\mathbf{s}(\theta) = s_x\exp(-i\theta)$.

After correlation, equations (A-5) and (A-6) become

$$\begin{aligned} C_{x+}(f) &= (T_{xx}(f) + iT_{xy}(f))\exp(-i\theta), \\ C_{x+}(f) &= (T_{yx}(f) + iT_{yy}(f))\exp(-i\theta), \\ C_{x-}(f) &= (T_{xx}(f) - iT_{xy}(f))\exp(i\theta), \\ C_{x-}(f) &= (T_{yx}(f) - iT_{yy}(f))\exp(i\theta). \end{aligned} \tag{B-2}$$

Consider the equation for $C_{x+}(f)$:

$$\begin{aligned} C_{x+} &= (T_{xx}(f) + iT_{xy}(f))(\cos(\theta) - i\sin(\theta)), \\ &= (T_{xx}(f)\cos(\theta) + T_{xy}(f)\sin(\theta)) \\ &\quad + i(-T_{xx}(f)\sin(\theta) + T_{xy}\cos(\theta)), \\ &= T_{xx'}(f) + iT_{xy'}(f), \end{aligned} \tag{B-3}$$

where we have introduced the coordinate system x', y' such that x' points along the direction of the source monitor sensor and y' is perpendicular to x'. Applying this procedure to all of equation (B-2), after correlation we have

$$\begin{aligned} C_{x+}(f) &= T_{xx'}(f) + iT_{xy'}(f), \\ C_{x+}(f) &= T_{yx'}(f) + iT_{yy'}(f), \\ C_{x-}(f) &= T_{xx'}(f) - iT_{xy'}(f), \\ C_{x-}(f) &= T_{yx'}(f) - iT_{yy'}(f), \end{aligned} \tag{B-4}$$

and, solving for the Ts,

$$\begin{aligned} T_{xx'}(f) &= (C_{x+}(f) + C_{x-}(f))/2, \\ T_{xy'}(f) &= -i(C_{x+}(f) - C_{x-}(f))/2, \\ T_{yx'}(f) &= (C_{y+}(f) + C_{y-}(f))/2, \\ T_{yy'}(f) &= -i(C_{y+}(f) - C_{y-}(f))/2. \end{aligned} \tag{B-5}$$

The right-hand sides of these equations are measured quantities; they are the x and y receivers and the source sensor signals for both ccw and cw rotations of the source. We use the source sensor signals to correlate the x and y receiver signals. This gives the earth response of two linear sources directed along and perpendicular to the direction of the source sensor, i.e., along x' and y'. The source sensor is rotated by an angle θ relative to the receiver x and y directions. Thus, the response tensor has components in both the receiver (x, y) and the source (x', y') coordinate systems. Since the source (x', y') coordinate system changes with different source positions, we need to rotate the source coordinates to the consistent receiver (x, y) coordinate system.

If we knew the direction θ, then we could rotate the source coordinate system so that it coincided with the receiver coordinate system. There are at least two ways to measure the angle θ: we could use another tool such as a compass or gyroscope to keep track of the rotation of the source, or we could determine the angle from the data as outlined in the main text.

To determine the angle as outlined in the main text, we assume we know the orientation of the receiver. If the receiver is also downhole, we have the same problem orienting the receiver as the source. Fortunately, we can determine the source angle using the vertical component of a three-component receiver. If we carry through the above analysis on a vertical receiver, we find

$$\begin{aligned} T_{zx'}(f) &= (C_{z+}(f) + C_{z-}(f))/2, \\ T_{zy'}(f) &= -i(C_{z+}(f) - C_{z-}(f))/2. \end{aligned} \tag{B-6}$$

By applying the rotation technique described in the text to the P-wave first-break wavelet, the angle necessary to rotate to the x, y coordinate system can be determined and applied to all three components. Thus, the orbital vibrator source and a three-component receiver will have a consistent coordinate system for all depth levels.